NASA Technical Memorandum 81213

AVRADCOM Technical Report 80-A-11

Comparison of Calculated and Measured Helicopter Rotor Lateral Flapping Angles

Wayne Johnson

July 1980

National Aeronautics and Space Administration

United States Army Aviation Research and Development Command

NASA Technical Memorandum 81213

AVRADCOM Technical Report 80-A-11

Comparison of Calculated and Measured Helicopter Rotor Lateral Flapping Angles

Wayne Johnson, Aeromechanics Laboratory
AVRADCOM Research and Technology Laboratories
Ames Research Center, Moffett Field, California

National Aeronautics and
Space Administration

Ames Research Center
Moffett Field, California 94035

United States Army
Aviation Research and
Development Command
St. Louis, Missouri 63166

COMPARISON OF CALCULATED AND MEASURED HELICOPTER ROTOR LATERAL FLAPPING ANGLES

Wayne Johnson*

U.S. Army Research and Technology Laboratories (AVRADCOM)
NASA, Ames Research Center
Moffett Field, California

ABSTRACT

Calculated and measured values of helicopter rotor flapping angles in forward flight are compared for a model rotor in a wind tunnel and an autogiro in gliding flight. The lateral flapping angles can be accurately predicted when a calculation of the nonuniform wake-induced velocity is used. At low advance ratios, it is also necessary to use a free wake geometry calculation. For the cases considered, the tip vortices in the rotor wake remain very close to the tip-path plane, so the calculated values of the flapping motion are sensitive to the fine details of the wake structure, specifically the viscous core radius of the tip vortices.

---

*Head of Rotorcraft Research Section, Large Scale Aerodynamics Branch

INTRODUCTION

The blades of an articulated helicopter rotor have a hinge at the blade root that allows out-of-plane motion called flapping. In forward flight a once-per-revolution motion of the blade about the flap hinge is produced, that corresponds to longitudinal and lateral tilt of the rotor tip-path plane relative to the shaft. Such motion occurs with hingeless and bearingless helicopter rotor designs as well, due to blade bending at the root rather than rotation about a flap hinge. The simplest analyses of helicopter rotor behavior assume that the induced velocity distribution is constant over the rotor disk. In fact however, the induced velocity distribution is highly nonuniform, and the rotor blade flapping motion is quite sensitive to the inflow distribution. Consider a longitudinal gradient of the induced velocity, increasing from the leading edge to the trailing edge of the rotor disk. The blade lift produced by such a distribution will be greater on the front of the disk than on the rear, so the rotor will be subjected to a longitudinal aerodynamic moment. An articulated rotor responds to this moment like a gyro, so the tip-path plane tilts laterally, toward the advancing side. Similarly a lateral inflow variation will produce a roll moment on the rotor, and hence a longitudinal tip-path plane tilt. With a hingeless rotor, the magnitude of the flapping response to nonuniform inflow is not greatly affected, but the phase of the response can be significantly decreased, so that a longitudinal inflow variation can produce longitudinal flapping as well as lateral flapping. Because of this sensitivity to the induced velocity distribution, it is difficult to calculate rotor blade flapping in forward

flight. An accurate calculation of flapping is needed in order to predict longitudinal and lateral cyclic control positions, particularly for new helicopter designs. Moreover, since the blade flap motion represents the integrated effect of the 1/rev aerodynamic environment of the rotor, difficulties in calculating it have serious implications regarding the predictive capability of rotor aerodynamic analyses in general.

In 1934, Wheatley[1] extended the theory of Glauert and Lock for the calculation of helicopter rotor forces and blade motion in forward flight. He evaluated the accuracy of the theory by comparing with flight test results for a Pitcairn autogiro in a glide. The rotor angle-of-attack, rotational speed, thrust coefficient, and longitudinal flapping angle were predicted with good accuracy, up to an advance ratio of about 0.4 or 0.5. The prediction of the lateral flapping angle was consistently low however. Wheatley identified the use of uniform inflow as the most critical assumption of the analysis. The sensitivity of the lateral flapping calculation to nonuniform inflow was demonstrated by using an induced velocity distribution that varied linearly from the leading edge to the trailing edge of the rotor disk. With such a longitudinal inflow variation, the prediction of the lateral flapping was improved, but was still significantly low (for an amplitude of the variation equal to 50% of the mean value). Wheatley concluded that the rotor blade flap motion can not be rigorously calculated without an accurate determination of the wake-induced inflow velocities.

In 1972, Harris[2] conducted a wind tunnel test of a model helicopter rotor, to examine the influence of advance ratio, thrust, and shaft

angle-of-attack on the rotor flapping angles. He found a large discrepancy between the measured lateral flapping and the values calculated using uniform inflow. Longitudinal flapping was estimated fairly well using uniform inflow, as were the trends with thrust and shaft angle. By using a nonuniform induced velocity calculation based on undistorted wake geometry, the prediction of lateral flapping was improved, but the measured results were still significantly underestimated at low advance ratio. Harris suggested that the primary source of the remaining discrepancy was the use of undistorted wake geometry.

The conclusions of Wheatley and Harris have remained conjectural. It is the purpose of this paper to examine the influence of nonuniform inflow and wake geometry on the calculation of helicopter rotor lateral flapping angles. The intent also is to establish the adequacy of the wake model in a helicopter rotor analysis, to the exter that may be inferred by comparisons with measurements of blade flapping motion.

ANALYTICAL MODEL

The rotor flapping motion was calculated using the helicopter analysis described in reference 3. The wake analysis was based on a discrete element representation of the vorticity, with models for the wake rollup and distorted wake geometry. The free wake geometry was calculated using the analysis of reference 4. The blade aerodynamic loading was calculated using lifting line theory, with corrections for three-dimensional effects at the tip and at blade-vortex interactions. The rotor blade flap motion was calculated by means of a harmonic analysis method. Rigid body flap

motion was the only degree of freedom considered. Four harmonics of the blade motion were calculated, using an azimuthal increment of 15°. Including blade lag motion, bending motion, or up to 10 harmonics in the calculation had little effect on the tip-path plane tilt. The effects of the blade torsion motion are discussed later in the paper. The flap motion relative to the shaft may be written as a Fourier series:

$$\beta = \beta_0 + \beta_{1c}\cos\psi + \beta_{1s}\sin\psi + \text{higher harmonics}$$

Here β_{1c} is the longitudinal tilt angle of the tip-path plane relative to the shaft, positive for forward tilt; β_{1s} is the lateral angle, positive for tilt toward the retreating side of the disk; and ψ is the blade azimuth angle, measured from downstream. If there is no cyclic pitch, both β_{1c} and β_{1s} will be negative in forward flight.

The induced velocity, circulation, and lift were evaluated at 15 stations along the blade, concentrated toward the tip. The trailed vorticity in the wake directly behind the blade was represented by discrete vortex lines positioned midway between the points at which the circulation was calculated. The strength of each trailed line was defined by the difference between the bound circulation at successive radial stations. This part of the model is a common numerical implementation of lifting line theory. For the rotary wing it is necessary also to model the rollup of the vorticity into a concentrated tip vortex, because the blade encounters the wake from the preceding blades as it rotates. Therefore, after an azimuthal extent of 30° in this case, the trailed vorticity was concentrated into a single tip vortex line, with strength equal to the maximum bound circulation of the blade. For conservation of vorticity,

there must be an inboard sheet of trailed vorticity with equal total strength and opposite sign as the tip vortex. This inboard sheet is much less important that the tip vortex, partly because the vorticity is not as concentrated and partly because it tends to be convected downward faster than the tip vortex. Consequently the entire inboard sheet could be reasonably represented by a single vortex line, with a large core radius (about 45% of the rotor radius in this case) to avoid unrealistically large induced velocities when the wake passed under the following blade. The bound circulation in forward flight varies azimuthally as well as radially, so the shed wake must also be included. The shed wake was modelled by radial, discrete vortex lines (also with a large core radius). A similar wake model was used for the other blades of the rotor. The detailed near wake model need not be used for these other blades since it is far from where the induced velocity is being calculated on the first blade. The curved trailed vortex elements in the wake are represented by a connected series of straight line segments, with an azimuthal increment of 15^{o} in this case. The vorticity strength varied linearly along each vortex line element, both trailed and shed. Four revolutions of the wake behind each blade were modelled in this fashion. It was determined that three revolutions were sufficient, except at the very lowest advance ratio analyzed.

A distributed vorticity model was used for the tip vortex core, in which one-half the vorticity was outside the core radius (defined at the point of maximum tangential velocity). With this model, the maximum velocity induced by the vortex was half that of a vortex with all the vorticity concentrated inside the core radius.

An undistorted wake geometry is obtained by assuming that each element of vorticity in the wake is convected downward at a rate equal to the mean induced velocity over the rotor disk, as the blades rotate and the helicopter flies forward. The resulting geometry consists of skewed, interlocking helices, one behind each blade. The self-induced distortion of the wake is neglected in this model. The analysis of reference 4 was used to calculate the distorted, free wake geometry in forward flight. The free wake geometry was calculated for the tip vortices only, for two revolutions of the wake behind each blade. Only two iterations within the free wake geometry calculation were necessary.

The analysis progressed in three stages. In the first stage, the blade motion and loading were calculated using uniform inflow. Next the wake influence coefficients were calculated with an undistorted wake geometry, and the motion and loading obtained using nonuniform inflow. Finally, the free wake geometry was calculated, the influence coefficients were re-evaluated, and the blade motion and loading again obtained using nonuniform inflow. It was determined that omitting any of these three stages gave unconverged results, but it was not necessary to repeat any stage before going on to the next. Within each stage, there was an iteration so that the calculated induced velocity and bound circulation were consistent. Also within each stage, there was an iteration on the collective pitch, in order to trim the rotor thrust to a prescribed value.

COMPARISON WITH WIND TUNNEL DATA

Harris measured the flapping angles of a model rotor in a wind tunnel. The principal parameters defining the rotor and operating conditions are

Table 1. Rotor Parameters and Operating Conditions

	Model Rotor	Autogiro Rotor
Radius, R	0.832 m	6.86 m
Number of blades	4	4
Solidity, σ	0.0891	0.1037
Lock number	5.80	19.1
Flap hinge offset, e/R	0.0229	0.0125
Twist	-9.14°	$5.^{\circ}$
Longitudinal cyclic	0.73°	0°
Lateral cyclic	0°	0°
Tip speed, ΩR	137. m/sec	102. m/sec
Nominal C_T/σ	0.080	0.064
Airfoil	V23010-1.58	Gottingen 429
Source of data	Reference 2	Reference 1

given in table 1. Complete details of the rotor and test data may be found in reference 2. An accuracy of $\pm 0.25^{\circ}$ is given for the flapping measurements. The wind tunnel had partly slotted walls, designed to produce no angle-of-attack change due to wall constraints, and the rotor diameter was only 27% of the tunnel width. Flow breakdown was estimated to occur at advance ratios below 0.04.

Figure 1 compares the calculated and measured values of the lateral flapping angle as a function of advance ratio, for a thrust coefficient to solidity ratio of 0.08 and a tip-path plane angle-of-attack of approximately 1° (aft tilt). For reference, a helicopter at an advance ratio of 0.15 would typically have a tip-path plane angle-of-attack of approximately 1° forward. The lateral flapping is underpredicted when uniform inflow is used, and even when nonuniform inflow based on the undistorted wake geometry is used. Below an advance ratio of about 0.16, it is necessary to include the free wake calculation in order to obtain a good estimate of the lateral flapping. Figure 2 shows the corresponding results for the longitudinal flapping angle, for which there is much less influence of the inflow model. The free wake geometry analysis was not applicable at hover and very low speed, so no calculated results are shown for advance ratios below 0.04. It was also found that the induced power calculation was significantly influenced by the wake model. Below an advance ratio of about 0.10, the calculated induced power was actually less than the ideal momentum theory value when the undistorted wake geometry was used, but was appropriately greater than the ideal value with the free wake geometry. For advance

ratios greater than 0.15, the calculated induced power was about the same for the two models.

Figure 3 shows the calculated vertical displacement of the tip vortices relative to the tip-path plane, for the two wake geometry models. The wake geometry is shown as a function of the wake age ϕ (the azimuth angle along the wake helix), for the rotor blade at four azimuth angles. The significant self-induced distortion of the free wake geometry is evident, resulting in numerous blade-vortex interactions in which the vertical separation is a fraction of the blade chord (which is 7% of the rotor radius). The tip vortices even pass above the blades initially, a behavior that has been observed experimentally as well.[5] Figure 4 shows the influence of the wake geometry on the calculated induced velocity. The discrete tip vortices of the rotor wake produce a 1/rev variation of the induced velocity that corresponds to a longitudinal gradient over the rotor disk, and hence increases the lateral flapping. By moving the wake closer to the tip-path plane, the induced velocity change on the sides of the disk, where the blades sweep over the tip vortices, is greatly increased. Consequently the wake geometry is an important factor in determining the lateral flapping at low advance ratio and low tip-path plane tilt.

In the cases considered here, the free wake geometry places the tip vortices so close to the blades that the calculated flapping is sensitive to the value of the viscous core radius, which determines the maximum velocity induced by the vortex. For the calculations presented in figures 1 to 4, a core radius of 0.05R was used. No measurements of the core radius are available for the model rotor being analyzed, so this value

was chosen based on the correlation produced. Figure 5 shows the sensitivity of the calculated induced velocity to the tip vortex core radius, and table 2 shows the corresponding calculated flapping angles. With the undistorted wake geometry, there is little influence of the core radius. These values of the vortex core radius should not be interpreted too literally however. There are a number of factors in addition to the core radius that combine to determine the magnitude of the vortex-induced loading, including the tip vortex stength, the extent of the tip vortex rollup, lifting surface effects on the induced blade loading, and possibly even vortex bursting or vortex-induced stall on the blade. In the absense of complete information about each of these phenomena, the vortex core radius is a convenient parameter with which to account for their cumulative influence on the rotor blade loading.

Figure 6 compares the measured and calculated values of the lateral flapping as a function of thrust, at an advance ratio of 0.08 and shaft angle of -1.35°. The free wake geometry is required to accurately predict the rate of change of β_{1s} with C_T/σ, and it is increasingly important at high thrust. Figure 7 compares the measured and calculated values of the lateral flapping as a function of the shaft angle-of-attack, at an advance ratio of 0.08 and a collective pitch of 11°.

In all cases, the collective pitch was adjusted to trim the calculated thrust to the measured value. It was found that the calculated collective pitch angles were consistently lower than the measured values, a common result in rotor analyses that may usually be attributed to elastic pitch

Table 2. Calculated influence of vortex core radius on blade flapping angles ($\mu = 0.1$, $C_T/\sigma = 0.08$, and $\alpha_{tpp} \cong 1^\circ$)

	Flapping Angles (deg) β_{1c}	β_{1s}
Free wake geometry		
core radius, r_c = 0.010R	-2.08	-4.17
0.030R	-2.47	-3.39
0.050R	-2.57	-3.13
0.075R	-2.56	-2.87
0.100R	-2.52	-2.68
Undistorted wake geometry		
core radius, r_c = 0.010R	-2.77	-1.69
0.030R	-2.73	-1.70
0.050R	-2.70	-1.70
0.075R	-2.66	-1.68
0.100R	-2.62	-1.65

deflection of the blade. Insufficient information was available regarding the physical characteristics determining the blade torsion dynamics (control system and blade stiffness, blade inertia and center-of-gravity distributions, and the aerodynamic center distribution) to allow an exploration of this facet of the analysis.

COMPARISON WITH FLIGHT DATA

Wheatley measured the flapping angles of an autogiro in gliding flight. The rotor and operating parameters are summarized in table 1; complete details of the aircraft and test data are given in references 1 and 6. An accuracy of $\pm 0.1^{\circ}$ is given for the flapping measurements. In the calculations the rotor was trimmed by setting the shaft angle-of-attack to the measured value, and adjusting the collective pitch to obtain the measured value of the rotor thrust coefficient. On an autogiro the rotor has a positive angle-of-attack (aft tilt of the tip-path plane), that becomes fairly large at low advance ratio.

Figure 8 compares the calculated and measured values of the lateral flapping as a function of advance ratio. Again it is essential to use nonuniform inflow in order to accurately predict the flapping angles, and below an advance ratio of about 0.20 it is also necessary to use the free wake geometry. Figure 9 shows the corresponding results for the longitudinal flapping, for which the influence of the nonuniform inflow is smaller but not negligible.

CONCLUDING REMARKS

Calculated and measured values of helicopter rotor flapping angles in forward flight have been compared for a model rotor in a wind tunnel and an autogiro rotor in gliding flight. It has been confirmed that the discrepancy between the experimental data and theories based on uniform inflow is attributable primarily to the highly nonuniform velocity induced at the blades by the tip vortices in the rotor wake. By using an analysis based on a calculation of the nonuniform inflow, it was possible to accurately calculate the rotor lateral flapping angles. At low advance ratios it is also necessary to use a free wake geometry, a result anticipated by Harris although not by Wheatley. The degree of sensitivity of an integrated effect of the rotor aerodynamic environment (the lateral flapping angle) to the fine structure of the wake is perhaps surprising, but plausible upon examination of the phenomenon. It is concluded that the principal features of the rotor wake are correctly represented in the nonuniform inflow and free wake geometry models utilized in this investigation. To correlate and develop these models further will require experimental data that encompasses the fine details of the rotor aerodynamics, such as measurements of the tip vortex circulation, core size, and peak velocities, even when the parameters of most interest are the integrated effects such as the first harmonic flapping motion.

REFERENCES

1. Wheatley, John B., "An Aerodynamic Analysis of the Autogiro Rotor with a Comparison between Calculated and Experimental Results," NACA Report No. 487, 1934
2. Harris, Franklin D., "Articulated Rotor Blade Flapping Motion at Low Advance Ratio," Journal of the American Helicopter Society, Vol. 17, No. 1, January 1972
3. Johnson, Wayne, "A Comprehensive Analytical Model of Rotorcraft Aerodynamics and Dynamics," NASA TM 81182, 1980
4. Scully, M.P., "Computation of Helicopter Rotor Wake Geometry and its Influence on Rotor Harmonic Airloads," Massachusetts Institute of Technology, ASRL TR 178-1, March 197_
5. Simons, I.A., Pacifico, R.E., and Jones, J.P., "The Movement, Structure, and Breakdown of Trailing Vortices from a Rotor Blade," CAL/AVLABS Symposium, Buffalo, New York, June 196_
6. Wheatley, John B., "Wing Pressure Distribution and Rotor-Blade Motion of an Autogiro as Determined in Flight," NACA Report No. 475, 1934

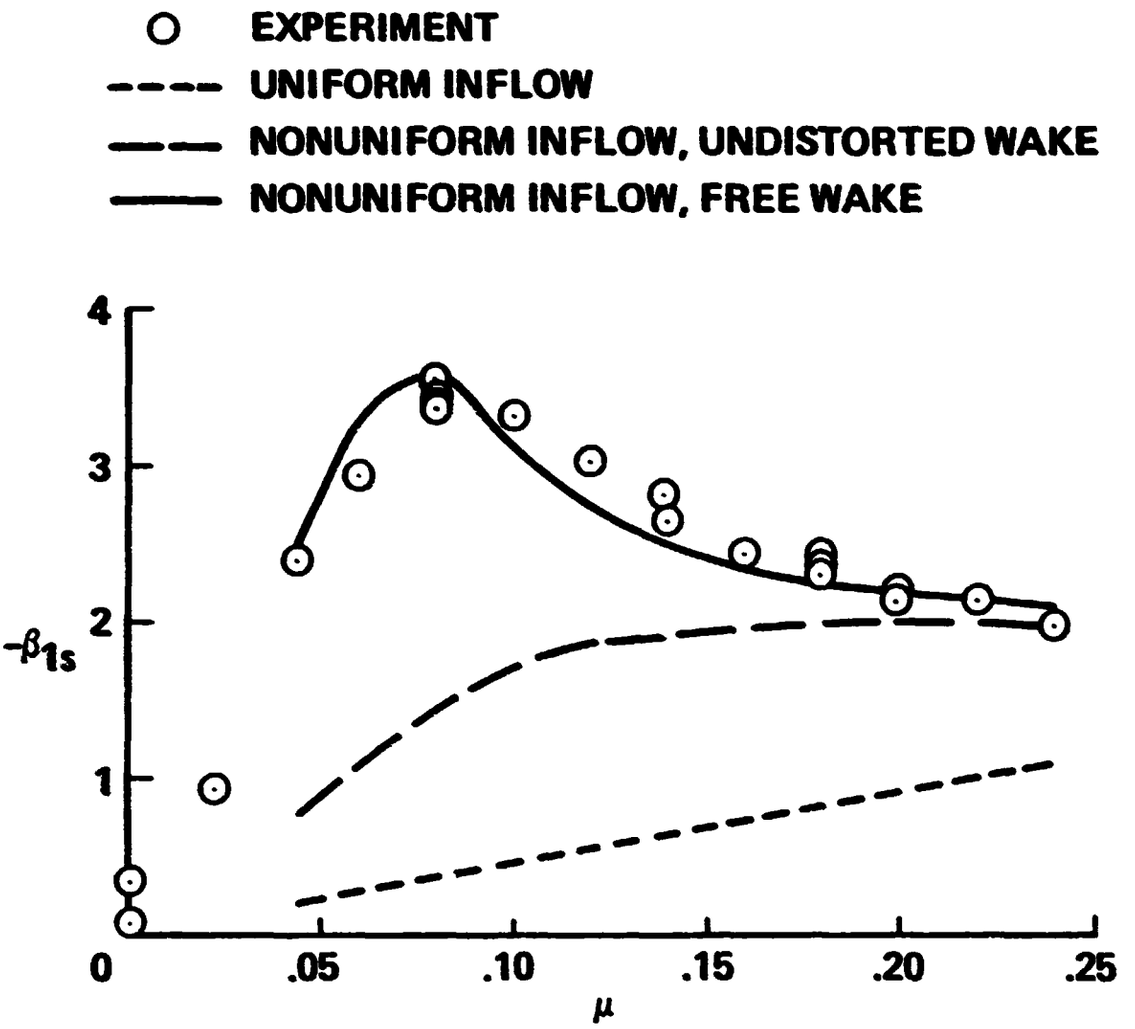

Figure 1. Comparison of measured and calculated model rotor lateral flapping angles as a function of advance ratio ($C_T/\sigma = 0.08$ and $\alpha_{tpp} \cong 1^\circ$)

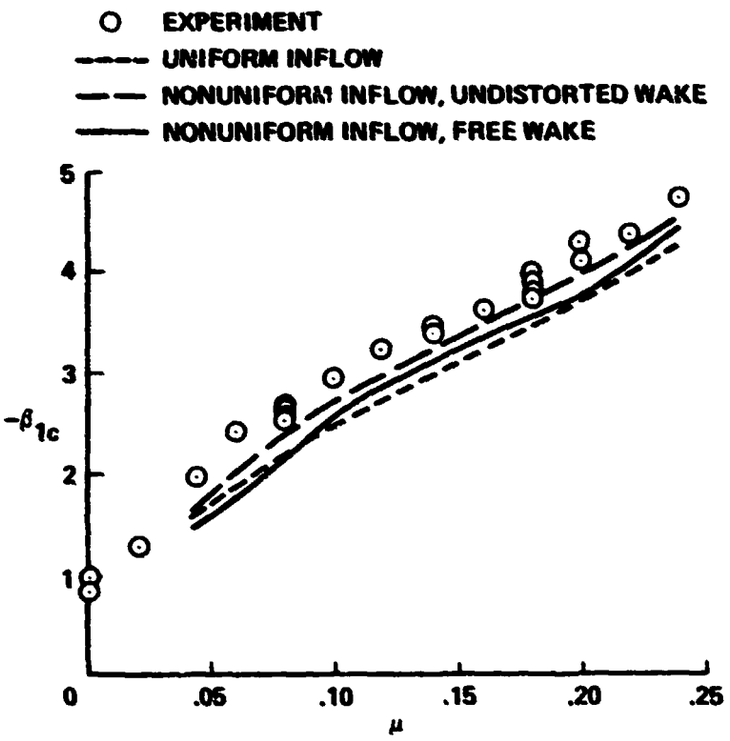

Figure 2. Comparison of measured and calculated model rotor longitudinal flapping angles as a function of advance ratio ($C_T/\sigma = 0.08$ and $\alpha_{tpp} \cong 1^\circ$)

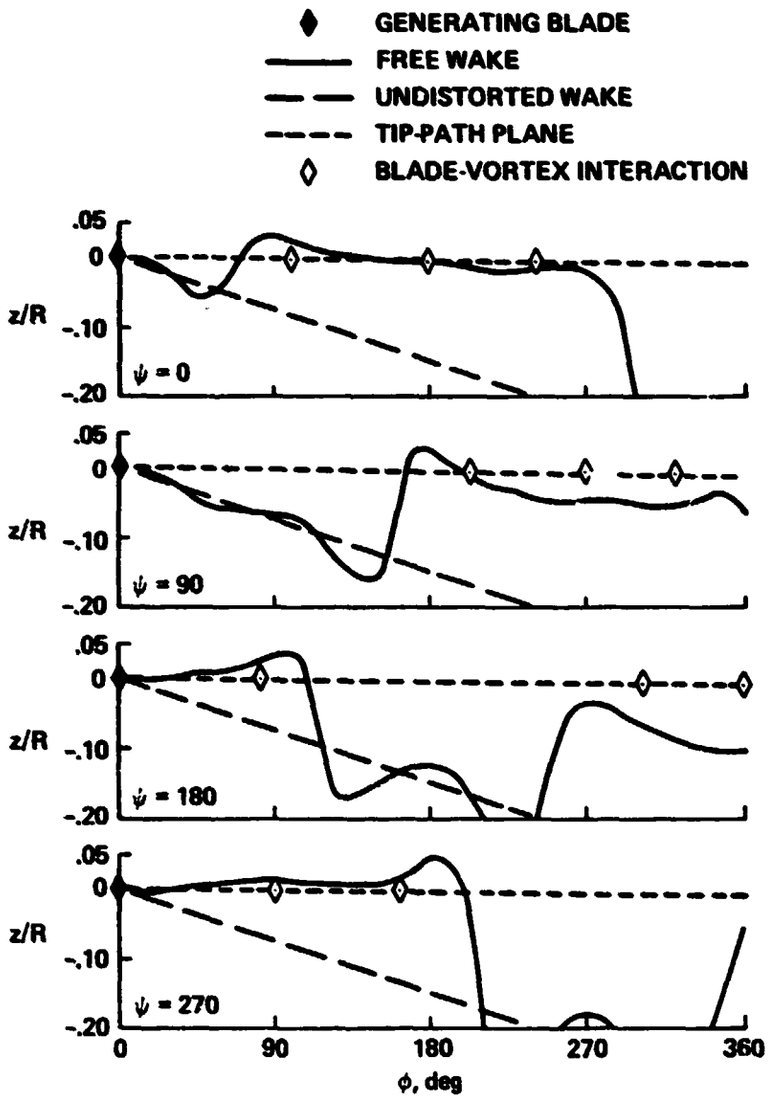

Figure 3. Calculated tip vortex vertical displacement ($\mu = 0.1$, $C_T/\sigma = 0.08$, and $\alpha_{tpp} \cong 1^\circ$)

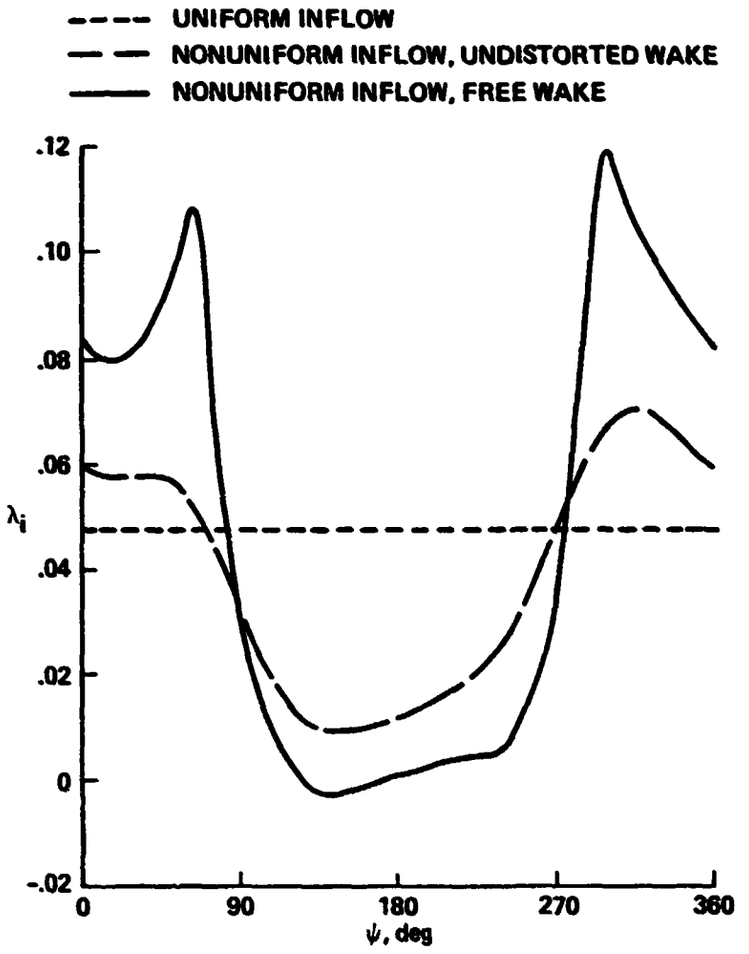

Figure 4. Calculated induced velocity at radial station $r/R = 0.92$ for the three wake models ($\mu = 0.1$, $C_T/\sigma = 0.08$, and $\alpha_{tpp} \cong 1^\circ$)

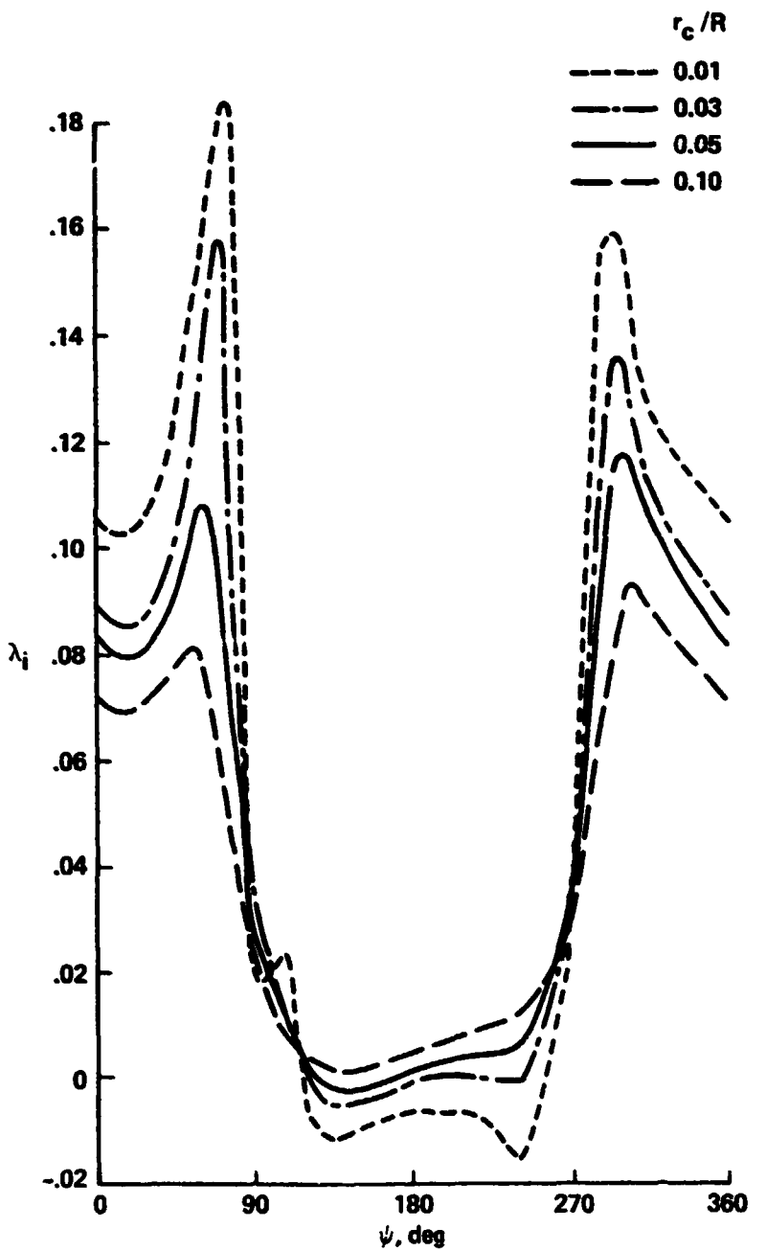

Figure 5. Calculated induced velocity at radial station r/R = 0.92 using the free wake model, as a function of tip vortex core radius ($\mu = 0.1$, $C_T/\sigma = 0.08$, and $\alpha_{tpp} \cong 1^\circ$)

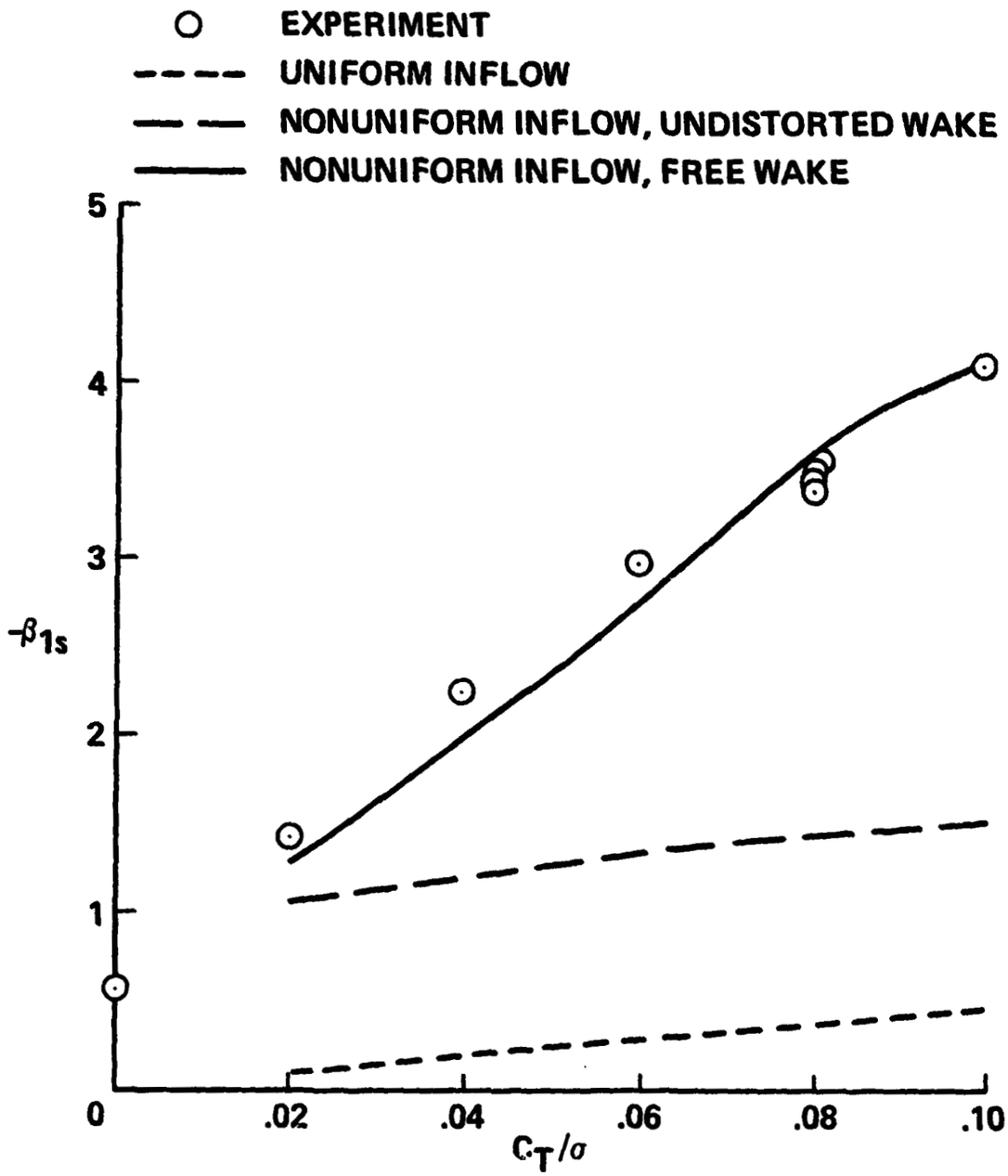

Figure 6. Comparison of measured and calculated model rotor lateral flapping angles as a function of thrust (μ = 0.08 and α_s = - 1.35°)

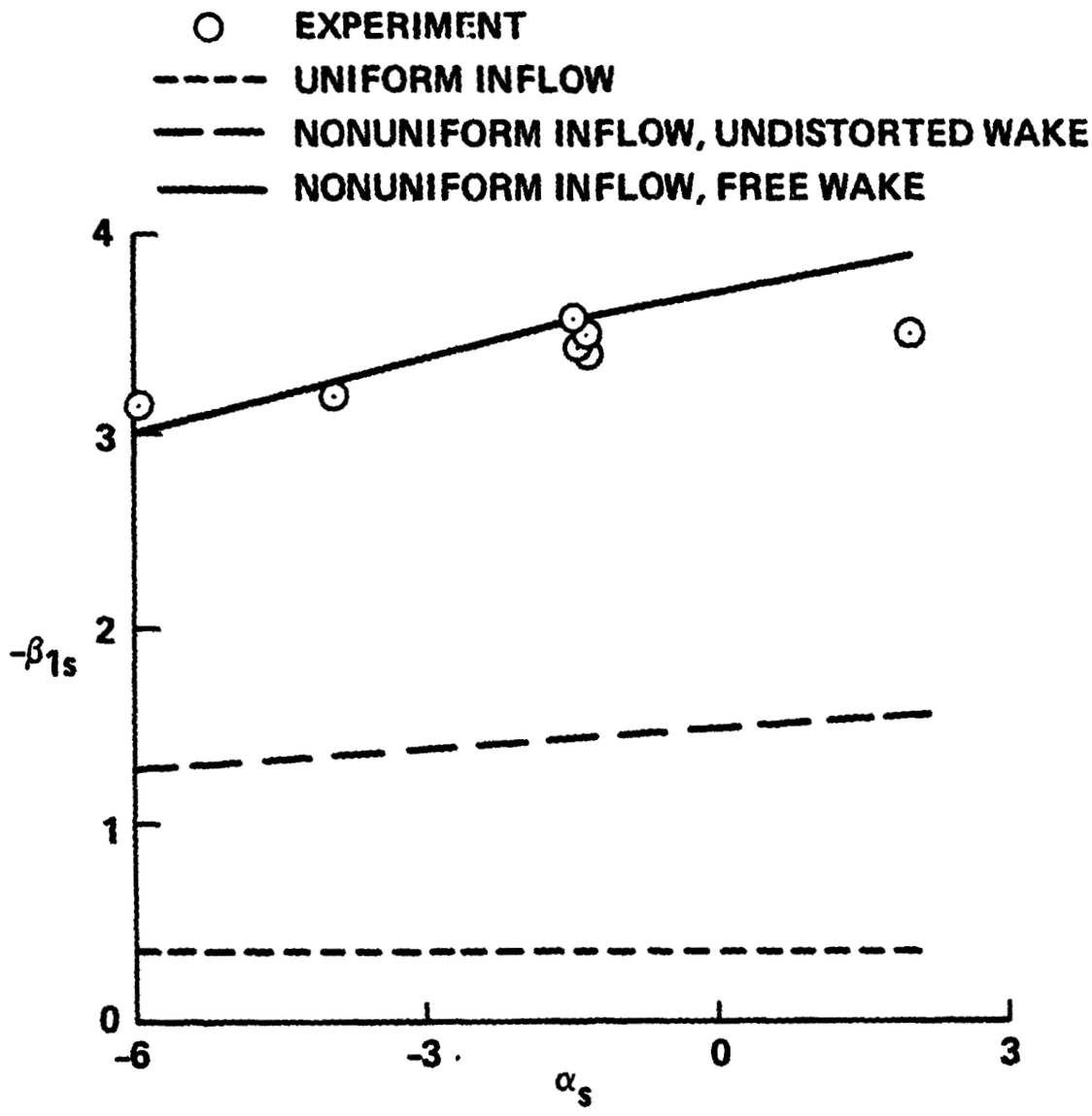

Figure 7. Comparison of measured and calculated model rotor lateral flapping angles as a function of shaft angle (μ = 0.08 and θ_{75} = 11°)

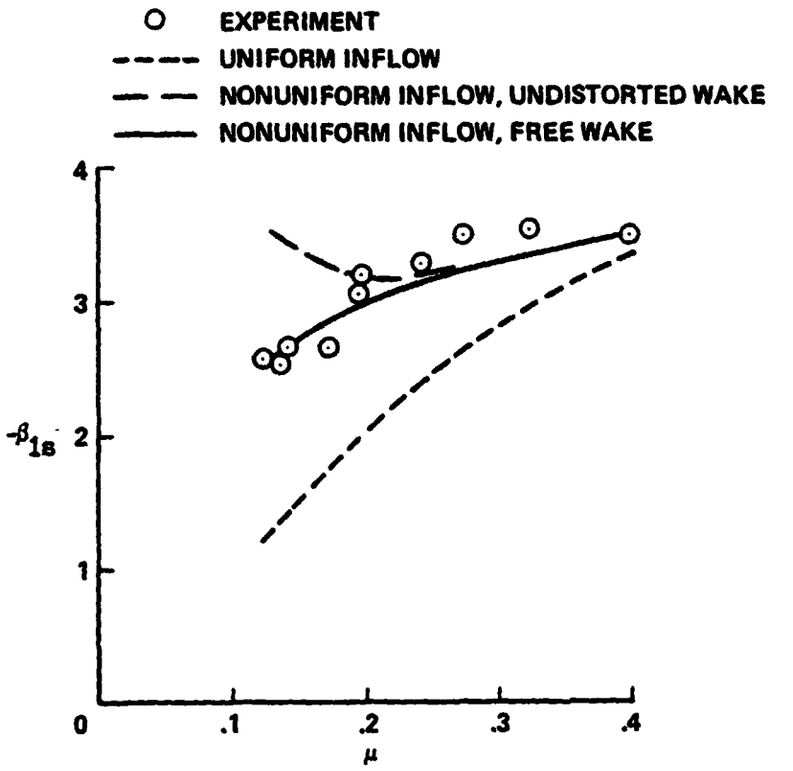

Figure 8. Comparison of measured and calculated autogiro rotor lateral flapping angles as a function of advance ratio